Separation and Purification Technology 368 (2025) 132980

Contents lists available at ScienceDirect

Separation and Purification Technology

journal homepage: www.elsevier.com/locate/seppur

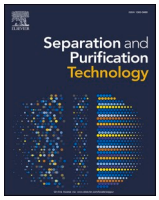

Additive manufacturing of ultrafiltration membranes from block copolymer nanowires

Jie Deng [a], Youxin Gong [a], Yang Jin [a], Jiemei Zhou [a,*], Yong Wang [a,b,**]

[a] State Key Laboratory of Materials-Oriented Chemical Engineering, College of Chemical Engineering, Nanjing Tech University, Nanjing 211816 Jiangsu, PR China
[b] School of Energy and Environment, Southeast University, Nanjing 210096 Jiangsu, PR China

ARTICLE INFO

Editor: Junyong Zhu

Keywords:
Additive manufacturing
Ultrafiltration
Polymerization-induced self-assembly
Block copolymers
Nanowires

ABSTRACT

Precise manipulation of the structure and performance of separation membranes holds immense significance for realizing highly efficient separations in ultrafiltration applications. Herein, we demonstrate an additive manufacturing approach to ultrafiltration membranes by controlled deposition of block copolymer nanowires on macroporous substrates via spray coating. The nanowires with a high concentration and good dispersibility are synthesized through in situ crosslinking polymerization-induced self-assembly. The nanowire morphology can be adjusted by changing the block ratio, enabling the selection of an optimal configuration for membrane preparation. By controlling the concentration and volume of deposited nanowires, intact separation layers composed of stacked nanowires can be formed. The thickness of the nanowire layer is directly correlated with the spraying parameters, and it shows great tunability within the range of approximately 100 nm–3 μm. This tunable thickness imparts adjustable separation performance to the resultant membranes. Furthermore, the strategy presented herein demonstrates exceptional up-scalability in the fabrication of ultrafiltration membranes, paving the way for industrial applications.

1. Introduction

Ultrafiltration is an important membrane separation technology that plays a pivotal role in ensuring the sustainable management of water resources, as it has widespread applications in water treatment and purification processes [1–3]. Ultrafiltration membranes have pore sizes ranging from 2 nm to 100 nm [4], which makes them highly effective for removing a wide range of contaminants from wastewater, such as viruses, microorganisms, colloidal particles, and natural organic matter, at low pressures [5–7]. However, the advancement of ultrafiltration membranes faces some choke points that limit the further enhancement of their performance and the expansion of the application areas [8–10]. The fabrication of ultrafiltration membranes is predominantly achieved through the nonsolvent-induced phase separation (NIPS) process, wherein the polymer solutions are immersed in the nonsolvent water to facilitate phase inversion [11,12]. This macroscopic phase separation process is highly sensitive to minor perturbations. Numerous factors, including solvent and nonsolvent types, polymer solution concentration, solvent-nonsolvent exchange, and environmental conditions, significantly influence membrane formation [13,14]. It is difficult to establish a clear and quantifiable relationship between these factors and the resulting membrane structure and properties. Furthermore, to enhance permeability and selectivity for efficient separation, post-modification or construction of composite membranes is a prevailing practice in the preparation of ultrafiltration membranes [15–17].

Currently, the integration of additive manufacturing with separation membrane preparation offers a promising approach to construct thin separation layers/functional layers with enhanced precision [18–22], thereby facilitating greater control over the structure and performance of separation membranes. Additive manufacturing, also known as 3-dimensional (3D) printing or rapid prototyping, is a technique that sequentially deposits 2D material layer-by-layer to form a 3D structure. It is more prevalent in fields of medicine, art, engineering and manufacturing initially, while has been extended to membrane fabrication and membrane modification in recent years [23–25]. Chowdhury et al [26] reported the additive approach, which combined the electrostatic spraying technology with the interfacial polymerization process, to deposit monomers directly onto a substrate, where they reacted

* Corresponding author.
** Corresponding author at: State Key Laboratory of Materials-Oriented Chemical Engineering, College of Chemical Engineering, Nanjing Tech University, Nanjing 211816, Jiangsu, PR China.
E-mail addresses: zhoujm@njtech.edu.cn (J. Zhou), yongwang@seu.edu.cn (Y. Wang).

https://doi.org/10.1016/j.seppur.2025.132980
Received 21 February 2025; Received in revised form 3 April 2025; Accepted 9 April 2025
Available online 10 April 2025

to form polyamide nanofiltration membranes. This approach allowed for fine regulation of the separation layer structure in thickness and roughness, giving a better desalination performance of the resulting membranes. Geng et al. [27] and Wang et al. [28] integrated electrostatic spraying with surface coating technology to develop a polydopamine surface coating on ultrafiltration membranes. This approach addressed issues such as the prolonged modification time associated with traditional polydopamine dip-coating methods, challenges in controlling the structure and composition of the modified layer, and the production of organic wastewater. Furthermore, it enables the precise regulation of the separation performance of ultrafiltration membranes. Whereafter, our group [29] sprayed carbon nanotubes on macroporous substrates. Assembled carbon nanotubes formed separation layers with flexibly tunable thicknesses, displaying fast removal of viruses and bacteria. These works designate that spray deposition of raw materials through additive approaches could be an effective way for fabricating separation membranes. The characteristics of raw materials therein crucially determine the viability of the approach. These materials should exhibit reactive or functional properties tailored to actual needs. Furthermore, low-dimensional nanoscale materials are preferred, as they can be intricately engineered into planar or 3D structures featuring nanopores that are suitable for ultrafiltration.

Regarding the preparation of low-dimensional nanoscale materials, considerable efforts have been made, yet most approaches only yield materials with low concentrations and involve intricate procedures [30–32]. However, it is essential to develop simple methods that can provide sufficient quantities of nanomaterials to serve as the raw materials for the preparation of membranes. In this context, polymerization-induced self-assembly (PISA) has been demonstrated to be a robust strategy for the fabrication of various polymeric nanomaterials from block copolymers (BCPs), including spherical micelles, nanowires, lamellae and vesicles [33,34]. The morphology of obtained nanomaterials can be flexibly regulated by adjusting the feed ratio, properties of the solvent, and the length ratio of blocks [35–37]. More importantly, PISA enables one-pot polymerization using environmentally friendly solvents like alcohols or water as solvents, leading to highly concentrated dispersions of nanomaterials (20–40 wt%) [38–40]. Consequently, the PISA approach facilitates the large-scale and eco-friendly production of nanomaterials. On this basis, we propose to fabricate nanomaterials via PISA and then deposit them onto the substrate through additive manufacturing to prepare ultrafiltration membranes, as shown in Scheme 1. In this work, the nanowires were specifically selected over other morphologies because they have a high aspect ratio and a large specific surface area. These properties facilitate the formation of tightly assembled, high-density, interconnected fine pores, which function effectively as sieving gates for efficient separations. Spray coating was employed to deposit the nanowires onto macroporous substrates, where the nanowires were stacked to form the separation layer. The resulting ultrafiltration membranes demonstrated adjustable permeance and rejections by changing the spraying parameters.

2. Experimental section

2.1. Materials

2-(Dimethylamino)ethyl methacrylate (DMAEMA, 99 %) and benzyl methacrylate (BzMA, 98 %) were procured from Aladdin, and 1,6-hexanediol bismethacrylate (HBMA, 97 %) was sourced from Macklin. These compounds were purified by passing through an alkaline oxidation alumina column to eliminate polymerization inhibitors, and subsequently stored in a refrigerator for later use. 2,2′-Azobis(2-methylpropionitrile) (AIBN, 99 %) was obtained from Aladdin and underwent recrystallization using ethanol prior to use. 2-Cyano-2-propyldithiobenzoate (CPDB, >97 %), ethanol (99.7 %) and tetrahydrofuran (THF, ≥99.9 %) were acquired from Aladdin without further purification. Petroleum ether (98 %) was supplied by Sinopharm Chemical Reagent Co., Ltd. The macroporous polyethersulfone (PES) membranes with an average pore size of 0.22 μm were purchased from Haining Yibo Filtration Equipment Co., Ltd and used as supporting substrates to fabricate ultrafiltration membranes. Orange II sodium salt (Biological stain) was purchased from Aladdin. Bovine serum albumin (BSA) and phosphate-buffered saline (PBS) sheets were purchased from MP Biomedicals Co., Ltd. Monodispersed gold nanoparticles with an aqueous colloidal size of 15 nm were obtained from BBI Solutions. Deionized water utilized in all experiments was prepared in the laboratory with an electrical conductivity range of 8–20 μS cm^{-1}.

2.2. Synthesis of BCP nanowires

The typical synthesis procedure of BCP nanowires was as follows. DMAEMA (4.716 g, 30 mmol), CPDB (221 mg, 1 mmol), AIBN (32.8 mg, 0.2 mmol), and THF (4 g) were mixed and placed in a polymerization tube equipped with a magnetic bar. After subjecting the tube to three

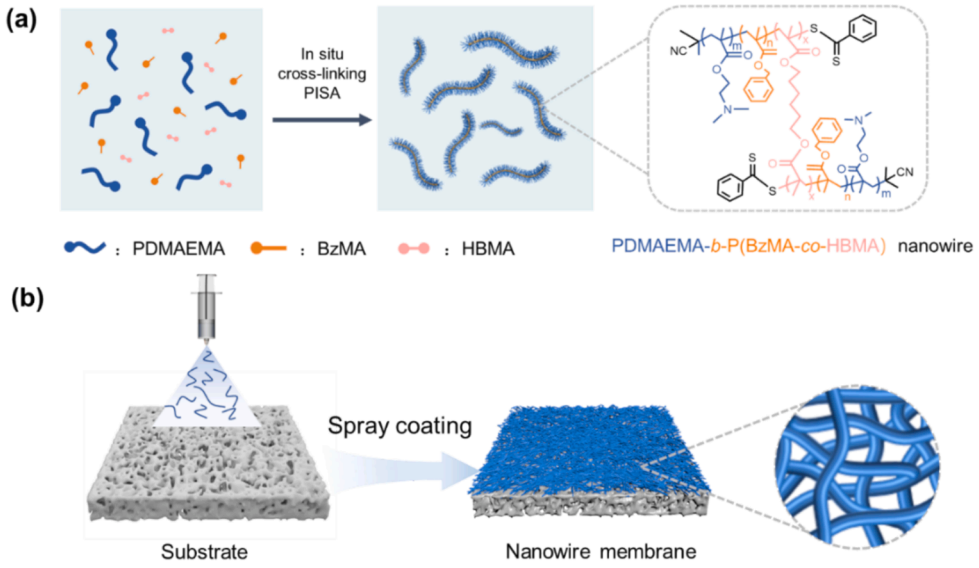

Scheme 1. Schematic diagram of the manufacturing process of nanowire membranes: (a) preparation of BCP nanowires via PISA and (b) additive manufacturing of membranes by spray coating of nanowires on the macroporous substrate.

cycles of liquid nitrogen freezing-vacuum-thawing, it was sealed and immersed in a 70 °C oil bath for 12 h. Upon completion of the reaction, the polymerization tube was cooled down to room temperature and opened to the air. The resulting polymer solution was then diluted with THF and precipitated to excess petroleum ether three times to eliminate any unreacted monomers. Subsequently, the polymer was dried at room temperature for 24 h in a vacuum drying oven, yielding a pink solid polymer of PDMAEMA-CPDB.

The synthesized PDMAEMA-CPDB was used as the macromolecular chain transfer agent for subsequent RAFT dispersed polymerization. A typical polymerization with a feed molar ratio of BzMA/PDMAEMA-CPDB = 70/1 and 20 wt% concentration was introduced here. PDMAEMA-CPDB (0.5 g, 0.101 mmol), BzMA (1.244 g, 7.07 mmol), HBMA (77 mg, 0.303 mmol), and AIBN (3.3 mg, 0.0202 mmol) were dissolved in ethanol (7.297 g). The solution was then blended and transferred to a polymerization tube with a magnetic bar. After degassing, the tube was sealed and placed in an oil bath at 70 °C for 16 h. Finally, the resultant dispersion solution of PDMAEMA-*b*-P(BzMA-*co*-HBMA) nanowires was transferred to a glass bottle for storage.

2.3. Preparation of nanowire membranes

The PDMAEMA-*b*-P(BzMA-*co*-HBMA) nanowire dispersion with a 20 wt% concentration was diluted by ethanol to prepare a series of membrane-forming solutions with a concentration range of 0.05 wt% to 1 wt%. The PES membrane was cut into a size of 10 × 10 cm^2 and fixed on the plate of the spraying apparatus (SEV-300EDN, Suzhou Second Automation Equipment Co., Ltd.). The surface of the membrane was cleaned with dustproof paper to remove any dust particles, preventing any potential defects during spraying. The nanowire dispersion solution was put into the syringe of the spraying apparatus and spray-coated onto the surface of the PES substrate using compressed air at a pressure of 1 bar. The spraying volume was adjusted within the range of 25 –75 μL cm^{-2} and the spray nozzle was maintained 62 mm above the plate. As the nozzle moved back and forth repeatedly, an even layer of nanowires was deposited atop the PES substrate. After natural drying in a fume hood, the nanowire membrane was obtained. The nanowire membrane with a larger area (25 × 25 cm^2) was prepared under the same conditions as described above.

2.4. Characterization

The chemical structure of polymers was characterized by the nuclear magnetic resonance (NMR) spectrum performed on a Bruker AV400 NMR spectrometer with $CDCl_3$ as the solvent. Transmission electron microscopy (TEM) observations were conducted on a JEOL JEM-2100 Plus instrument with an accelerating voltage of 100 kV. The nanowire dispersion was subjected to ultrasonic treatment for 30 min and then dropped onto a copper grid. After ethanol evaporated naturally, the TEM sample was obtained for observation. The average diameter of the nanowire was analyzed using Image J software based on the TEM images. To ensure accuracy, at least 100 positions across images were measured to calculate the average value. The surface and cross-sectional morphologies of the nanowire membranes were characterized by field emission scanning electron microscopy (FESEM, Hitachi S-4800) with an accelerating voltage of 5.0 kV and an electric current of 7 mA. To prepare the cross-sectional sample, the nanowire membrane was immersed in liquid nitrogen and quickly fractured to reveal the cross-sectional structure. Prior to characterization, all samples were subjected to gold plating for 40 s to mitigate charging effects and improve imaging quality. The thickness of the nanowire layer was determined through the analysis of cross-sectional SEM images. At least five different locations on each sample were measured to get the average thickness value. The surface zeta potentials of nanowire membranes were examined by an electrokinetic analyzer (SurPASS Anton Paar, Austria). Water contact angle (WCA) measurements to analyze the surface hydrophilicity were performed using a contact angle goniometer (DropMeter A-100, Maist).

2.5. Filtration experiments

The separation performance of the nanowire membranes was evaluated by employing a dead-end filtration apparatus (Amicon 8003, Merck Millipore) under a pressure of 0.5 bar. Prior to measurement, the membrane was pre-compacted for 10 min under the same pressure to reach a stable filtration state. Water permeance (L m^{-2} h^{-1} bar^{-1}) was calculated using Eq. (1):

$$P = \frac{V}{A \cdot t \cdot p} \tag{1}$$

where *V (L)* represents the volume of water that permeates through the membrane over the testing duration *t* (h), *A* (m^2) represents the active filtration area, and *p* (bar) denotes the *trans*-membrane pressure during the test.

BSA and monodispersed gold nanoparticles with a diameter of 15 nm were employed to conduct the rejection tests of the nanowire membranes. To prevent the adsorption of gold nanoparticles on the membrane surface, the membranes were soaked in the orange II sodium salt solution (5 mg L^{-1}) for 20 min to neutralize the electrical property of the membrane surface. After pretreatment, the membrane surface would change from white to light yellow. The rejection rate (*R*) was determined using Eq. (2):

$$R = \frac{C_f - C_p}{C_f} \times 100\% \tag{2}$$

where C_p represents the concentration of gold nanoparticles or BSA in the permeation solutions, and C_f represents the concentration of gold nanoparticles or BSA in the feed solution. The concentration of gold nanoparticles or BSA was measured using a UV–visible spectrophotometer (NanoDrop 2000C, Thermo Fisher Scientific), based on the characteristic absorption peaks of gold nanoparticles at 520 nm and BSA at 280 nm.

In order to measure the molecular weight cut off (MWCO) of membranes, four kinds of dextrans with different molecular weights (10 kDa, 40 kDa, 70 kDa and 500 kDa) were dissolved in water to prepare a dextran mixed solution. The concentration of each dextran component above was 2.5 g L^{-1}, 1 g L^{-1}, 1 g L^{-1}, and 2 g L^{-1}, respectively. The dextran concentrations in the feed solution and the permeation solution were tested by gel permeation chromatography (GPC, Waters 1515). The effective pore size of membranes can be calculated by Eq. (3) [41]:

$$r = 0.33 {M_w}^{0.46} \tag{3}$$

where *r (Å)* is the effective pore radius of membranes and M_w *(Da)* is the MWCO of dextran.

3. Results and discussion

3.1. Synthesis of BCP nanowires

Polymer nanowires were fabricated through the strategy of in situ crosslinking PISA. First, RAFT polymerization of DMAEMA in THF was carried out using CPDB as a chain transfer agent to prepare the PDMAEMA-CPDB homopolymer (Fig. S1a). ^{1}H NMR spectrum confirmed the chemical structure of the product, with all characteristic signals corresponding to the protons in PDMAEMA-CPDB clearly identified, as shown in Fig. S2. The degree of polymerization of PDMAEMA ($DP_{PDMAEMA}$) was determined to be 29 based on the integral values of signals at 4.06 and 7.32–7.94 ppm, which belong to the ester methylene protons of DMAEMA units and the phenyl protons of CPDB. Then, PDMAEMA-CPDB served as the macro chain transfer agent to conduct

the polymerization of BzMA and HBMA in ethanol (Fig. S1b) for the preparation of BCP nanowires. Prior to polymerization, PDMAEMA and all monomers were thoroughly dissolved in ethanol, yielding a homogenous and transparent solution. As the polymerization progressed, the chain extension of PDMAEMA engendered a second insoluble block of PBzMA. The resultant amphiphilic block copolymer exhibited self-assembly behavior in ethanol, forming nano-objects with a solvophobic core composed of PBzMA stabilized by a solvophilic shell of PDMAEMA, leading to a heterogeneous dispersion solution. The presence of HBMA within the polymerization system facilitated the morphological evolution of nano-objects from spherical micelles to nanowires, simultaneously introducing crosslinking within the solvophobic blocks, which effectively inhibited further transformation into vesicles [42]. Consequently, this in situ crosslinking PISA process made the fabrication of nanowires more facile and controllable. The molar feed ratio of HBMA to PDMAEMA-CPDB was fixed at 3:1. The target DP_{PBzMA} was adjusted from 50, 60, 70, 80 to 90, and the corresponding PDMAEMA-*b*-P(BzMA-*co*-HBMA) nano-objects were designated as DBH-50, DBH-60, DBH-70, DBH-80, and DBH-90, respectively. As the solvophobic block PBzMA was progressively increased in length, the polymerization system underwent a remarkable transformation in apparent state. This evolution transitioned from a solution with increased viscosity, as observed in the progression from DBH-50 to DBH-70 (Fig. S3a–c), to the formation of bulk solids in DBH-80 and DBH-90 (Fig. S3d–e). TEM characterization was used to examine the morphologies of the obtained nano-objects as shown in Fig. 1. At $DP_{PBzMA} = 50$, spherical micelles with an average diameter of 30 nm were observed. In contrast, nanowires were formed at $DP_{PBzMA} = 60$, 70, 80, and 90. The increase in DP_{PBzMA} led to the longer solvophobic chains aggregated in the core of the nanowires, therefore their average diameters were increased from 18 nm, 20 nm, 25 nm, to 26 nm, respectively. SEM observation also revealed the morphologies at varying DP_{PBzMA} (Fig. S4), consistent with the results of TEM characterizations. In addition to the change in diameter, the nanowires at $DP_{PBzMA} = 80$ and 90 began to entangle with each other, forming a network structure. This phenomenon was strikingly apparent, as the polymerization system manifested as a blocky solid, which posed challenges for achieving effective dilution and homogeneous dispersion of nanowires in solvents, thereby complicating subsequent spray processing. DBH-60 and DBH-70 nanowires exhibited excellent dispersibility in ethanol, even at a quite high concentration of 20 wt% in the polymerization system. Therefore, DBH-60 and DBH-70 nanowires were chosen as the building blocks for the preparation of nanowire membranes.

3.2. Preparation of nanowire membranes

PDMAEMA-*b*-P(BzMA-*co*-HBMA) nanowires were readily deposited onto the surface of macroporous substrates due to their micrometer-long lengths, which enabled them to bridge across the substrate pores. These nanowires stacked upon one another and coalesced into a thin layer, with the interstices between the nanowires forming interconnected pores. The nanometer-scale diameter of the nanowires dictated that the interstices between them were correspondingly in the nanometer range. The hydrophilic PDMAEMA shell of nanowires could impart hydrophilic properties to the nanowire layer, facilitating water penetration, while the cross-linked P(BzMA-*co*-HBMA) cores could ensure structural stability. The nanowires at a high concentration were diluted tens to hundreds of times in ethanol, preparing low-concentration and homogeneous dispersions for subsequent spray coating (Fig. S5). The macroporous PES membrane was used as the supporting substrate. The original PES membrane presented a matte appearance, while the surface of the membrane became shiny after spray coating of nanowires (Fig. S6). To achieve a defect-free and uniform nanowire separation layer, we systematically investigated the spray coating parameters, specifically the sprayed concentration and volume of the nanowire dispersions. The DHB-70 nanowires were first employed, and the sprayed volumes were adjusted in 75, 50 and 25 μL cm^{-2}. The pristine PES substrate exhibited irregularly distributed large pores on the surface (Fig. S7). After spray coating of nanowires, it was evident that the nanowires fully covered the PES substrate surface. At concentrations of 1 wt% and 0.5 wt%, the deposited nanowires formed separation layers with thicknesses ranging from approximately 400 nm to 3 μm (Figs. S8 and S9). When the sprayed concentration was 1 wt%, the thicknesses at volumes of 75, 50 and 25 μL cm^{-2} were 3261 nm, 2980 nm and 1414

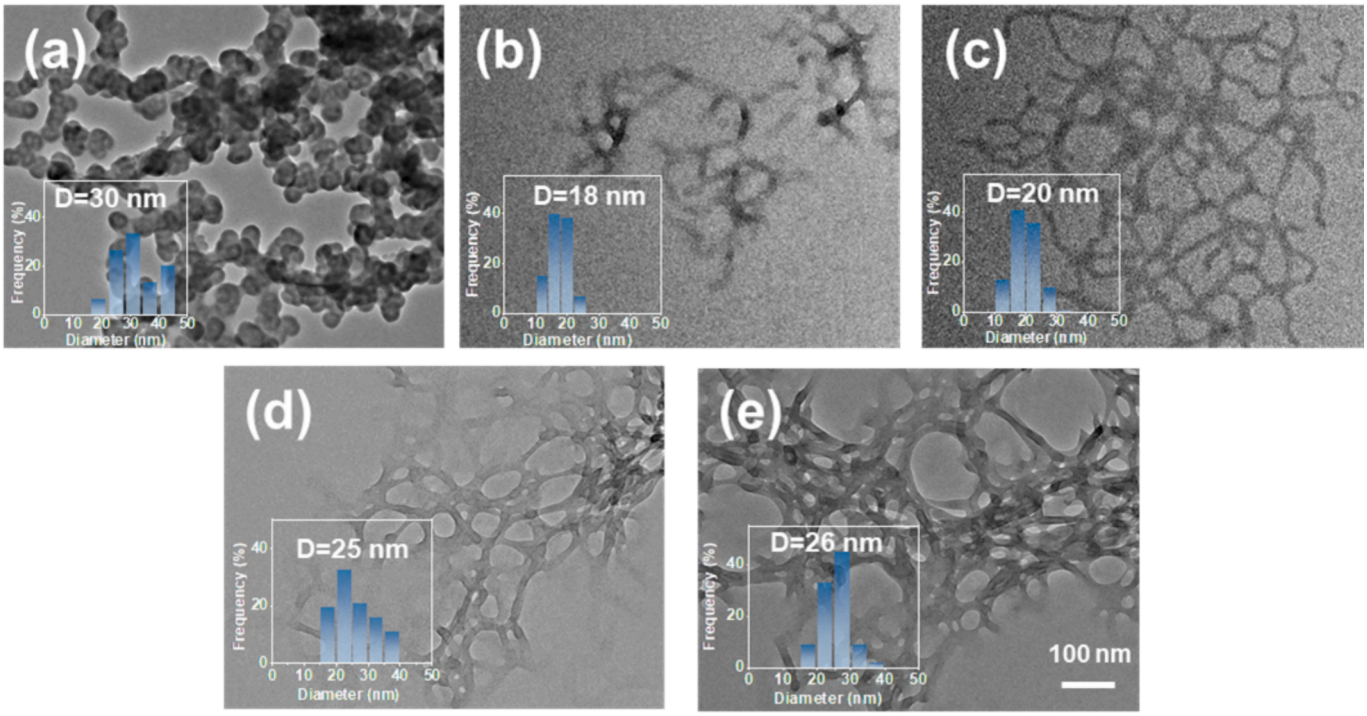

Fig. 1. TEM images of different DBH nano-objects: (a) DBH-50, (b) DBH-60, (c) DBH-70, (d) DBH-80 and (e) DBH-90. All images have the same magnification.

nm. For a concentration of 0.5 wt%, the thicknesses at volumes of 75, 50 and 25 μL cm^{-2} were 1542 nm, 994 nm, and 370 nm, respectively. In pursuit of thinner nanowire layers, we further decreased the sprayed concentration to 0.25 wt% for examination. It was observed that the complete nanowire layers were also formed on the substrate surface without exposing the porous PES (Fig. S8). When the sprayed volumes were 75, 50 and 25 μL cm^{-2-2}, the thicknesses of the nanowire layers were 835 nm, 577 nm and 318 nm, respectively (Fig. S9). Compared to the concentrations of 1 wt% and 0.5 wt%, the thicknesses had a certain decrease at the same sprayed volume. By changing the sprayed concentration to 0.1 wt% (Fig. 2a-f), the thicknesses of the nanowire layers were 243 nm, 198 nm, and 129 nm, corresponding to the sprayed volumes of 75, 50 and 25 μL cm^{-2}, respectively. At this concentration, the nanowire layer was very thin. The nanowires suspended over the macropores of the substrate membrane exhibited slight indentation due to the underlying macropores, leading to a mildly uneven surface. Nevertheless, the integrity of the nanowire layers was maintained without any discernible defects. Further reducing the sprayed concentration to 0.075 wt% (Fig. S10), it was found that the sprayed volume of 25 μL cm^{-2} was not sufficient to cover the substrate and form a complete membrane surface. Even when the sprayed volume was increased to 50 μL cm^{-2} and 75 μL cm^{-2}, abnormally large pores were still present on the surface of the PES substrate. These results indicate that by changing the sprayed concentrations from 1 wt% to 0.1 wt% and the sprayed volumes from 25 μL cm^{-2} to 75 μL cm^{-2}, we could precisely adjust the thickness of the nanowire layer in a range of about 100 nm to 3 μm, as shown in Fig. 2(g).

The morphology and performance of the BCP nanowire membrane are closely related to the diameter and length of the nanowires. Therefore, the spray coating parameters for DBH-60 nanowires were also investigated for the preparation of nanowire membranes. The DBH-60 nanowire dispersion with different concentrations was sprayed onto the surface of the PES substrate (Fig. S11). At a concentration of 1 wt%, the nanowire layers were formed with no defects or large pores. The thicknesses at sprayed volumes of 75, 50 and 25 μL cm^{-2} were 1538 nm, 1069 nm and 397 nm, respectively. Compared with DBH-70, the thickness of the DBH-60 nanowire layer was decreased significantly under the same spraying conditions. When the sprayed concentration was adjusted to 0.75 wt%, the sprayed volumes of 75 and 50 μL cm^{-2} could form a defect-free layer with a thickness of 1109 nm and 457 nm, respectively. However, decreasing the sprayed volume to 25 μL cm^{-2} was not enough to form a complete nanowire layer, and the porous structure of the PES substrate was exposed obviously. In comparison to the DBH-70 nanowire, a complete DBH-60 nanowire layer could only be achieved by increasing the concentration approximately tenfold. This phenomenon may be attributed to the smaller dimensions of the DBH-60 nanowire in both length and diameter relative to the DBH-70 nanowire, which made it easier to penetrate the PES substrate during the spraying process. Consequently, it was only at higher concentrations that the DBH-60 nanowire could accumulate sufficiently to form a complete and

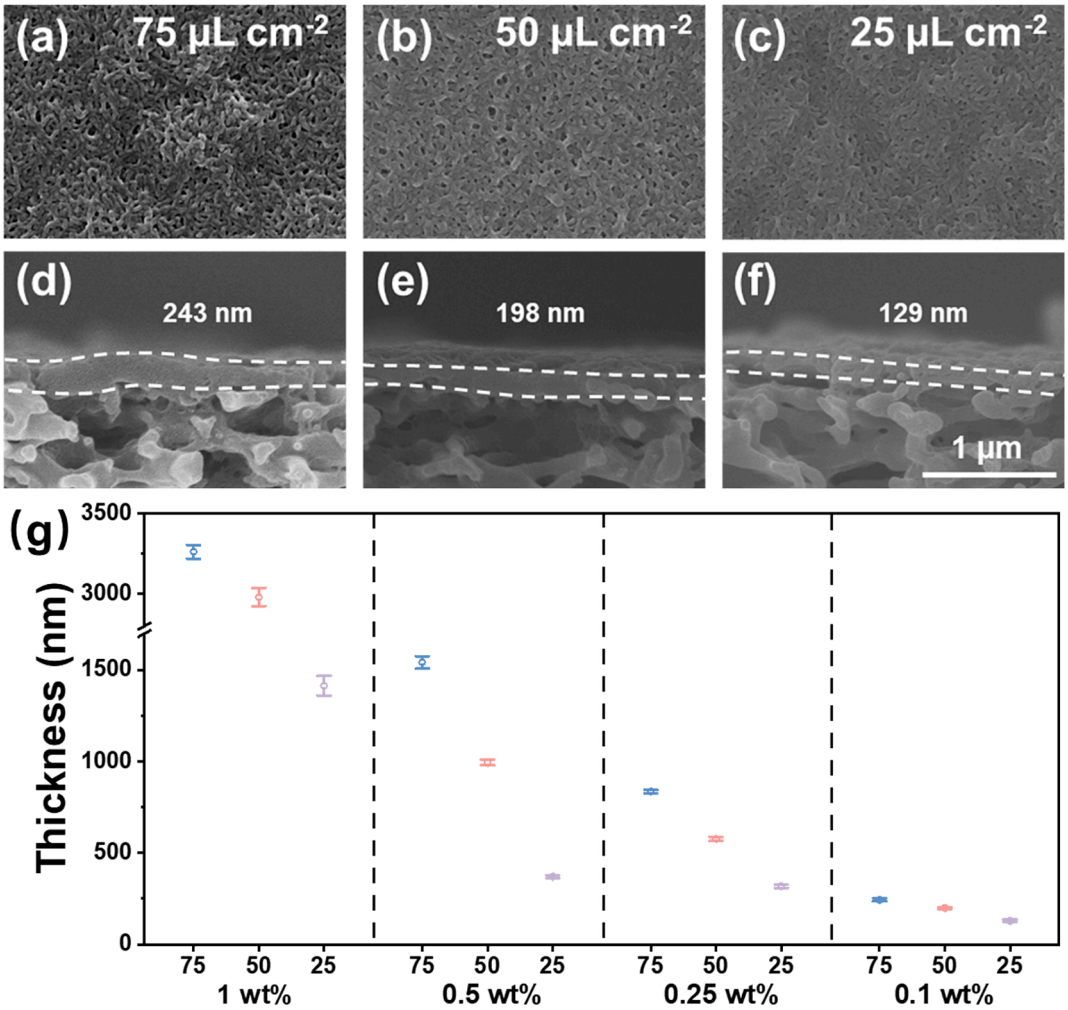

Fig. 2. (a–c) Surface and (d–f) cross-sectional SEM images of the DBH-70 nanowire membranes with different sprayed volumes at a concentration of 0.1 wt%. All images have the same magnification, and the scale bar corresponding to 1 μm is given in (f). (g) The thicknesses of the nanowire layers at a series of sprayed concentrations (1–0.1 wt%) and volumes (70–25 μL cm^{-2}).

robust structure. These observations suggest that the length and diameter of the nanowires have important effects on the spraying process and the DBH-70 nanowire is more suitable as the building block to prepare the nanowire membranes.

To investigate the surface properties of the prepared nanowire membranes, the surface zeta potential and WCA were measured as shown in Fig. 3. The surface zeta potential of the membranes changed from positive to negative as the pH was increased. The isoelectric point of the nanowire membrane was found to range between 6.8 and 7.7, with a corresponding increase in value observed as the sprayed nanowire concentration was elevated. Despite PDMAEMA chains (pKa = 7.2) being recognized as a weakly positively charged polymer, the nanowire membranes exhibited near-electric neutrality in water (pH = 7.4). This phenomenon may be attributed to the negatively charged PES substrate [43], which neutralized the weak positive charge of the nanowire. The WCA values for the nanowire membranes with sprayed concentrations of 1, 0.5, 0.25, and 0.1 wt% were determined to be 77°, 74°, 66°, and 53°, respectively, indicating their relative hydrophilicity. The decrease in WCA values with decreasing sprayed concentrations can be ascribed to enhanced surface porosity.

3.3. Ultrafiltration performance

The separation performances of the DBH-70 nanowire membranes prepared with different sprayed volumes and concentrations were tested as shown in Fig. 4. The water permeance of the membrane was gradually increased as the sprayed concentration was decreased. When the spray concentration was 1 wt% and 0.5 wt%, the water permeances of the nanowire membranes with 75, 50 and 25 μL cm^{-2} sprayed volumes were 52, 54, 107, 53, 71 and 220 L m^{-2} h^{-1} bar^{-1}. Reducing the sprayed concentration to 0.25 wt% and 0.1 wt%, the water permeances of the membranes corresponding to 75, 50 and 25 μL cm^{-2} sprayed volumes were increased to 242, 306, 394, 584, 825 and 1828 L m^{-2} h^{-1} bar^{-1}. During the performance test, the membrane thickness had a great influence on the mass transfer resistance. For the nanowire membrane, the nanowire layer functioned as the separation layer, whereas the substrate membrane's contribution was minimal due to its significantly larger pore sizes. Consequently, the thickness of the nanowire layer predominantly determined the permeance resistance. With the ever-decreasing amount of deposited nanowires, the effective thickness of the nanowire layer kept decreasing, thereby reducing mass transfer resistance and leading to a continuous increase in permeance from 52 to 1828 L m^{-2} h^{-1} bar^{-1}. In addition to the thickness, the pore size of the separation layer synergistically contributed to the permeance. At higher concentrations of the sprayed nanowire (1 wt% and 0.5 wt%), the packing density of nanowires remained robustly high, thereby the pore size of the nanowire layer had no significant change with the decreased thickness. Consequently, the permeance was increased slowly from 52 to 220 L m^{-2} h^{-1} bar^{-1}. At lower concentrations (0.25 wt% and 0.1 wt%), the packing of nanowires became loose and the pore size became larger with the decreasing concentration. Both the thickness reduction and enlarged pore size resulted in a pronounced escalation in permeance from 242 to 1828 L m^{-2} h^{-1} bar^{-1}.

Two model materials, BSA and 15 nm monodispersed gold nanoparticles, were utilized to investigate the separation capability of the membranes. BSA is an elliptical protein with a molecular weight of 66 kDa, whose dynamic diameter is about 6.8 nm [44]. When the sprayed concentration was 1 wt% and 0.5 wt%, the BSA rejection of the nanowire membranes with 75, 50 and 25 μL cm^{-2} sprayed volumes were 75 %, 71 %, 65 %, 66 %, 61 % and 50 %. Reducing the sprayed concentration to 0.25 wt% and 0.1 wt%, the BSA rejection of the membranes with 75, 50 and 25 μL cm^{-2} sprayed volumes were decreased to 59 %, 52 %, 43 %, 40 %, 35 % and 18 %. Normally, both size exclusion and electrostatic forces exert a profound influence on the retention of BSA. However, as evidenced by the surface zeta potential analysis (Fig. 3a), the nanowire membrane demonstrated near-neutral characteristics, effectively minimizing the electrostatic effect during the separation process. Consequently, the primary cause for the gradual decline in the BSA rejection lay in the reduced mass transfer resistance and the enlarged pore size. The other model material, the gold nanoparticle, is a spheroidal particle with a diameter of 15 nm. The rejections to the gold nanoparticle at the sprayed concentrations of 1 wt% and 0.5 wt%, and the sprayed volumes of 75, 50 and 25 μL cm^{-2}, were 98.9 %, 98.3 %, 97.2 %, 98.5 %, 97.9 %, and 96.9 %, respectively. At sprayed concentrations of 0.25 wt% and 0.1 wt%, the rejection rates were determined to be 96.3 %, 95.7 %, 95.2 %, 94.5 %, 92.2 % and 81.8 %, with sprayed volumes of 75, 50 and 25 μL cm^{-2}. To evaluate the change in effective pore size of the membranes with the sprayed concentrations, the MWCOs were determined by testing the membrane rejections to dextrans with varying molecular weights. When the sprayed concentrations ranged from 1 wt% to 0.1 wt% at a sprayed volume of 75 μL cm^{-2}, MWCOs of the corresponding membranes were found to be 55 kDa, 63 kDa, 89 kDa and 231 kDa, respectively. The effective pore sizes, calculated based on the MWCOs, were determined to be 10 nm, 10.7 nm, 12.5 nm and 19.4 nm, respectively. The membranes exhibited high rejections to the gold nanoparticle compared to that of BSA, because of the larger size of the gold nanoparticle. The detailed data about the thicknesses and separation performances of the nanowire membranes at a series of sprayed concentrations (1–0.1 wt%) and volumes (70–25 μL cm^{-2}) are summarized in Table S1 for convenient access. The separation performance of the nanowire membrane could be flexibly adjusted with the permeance in the range of about 50–1800 L m^{-2} h^{-1} bar^{-1}, the rejection

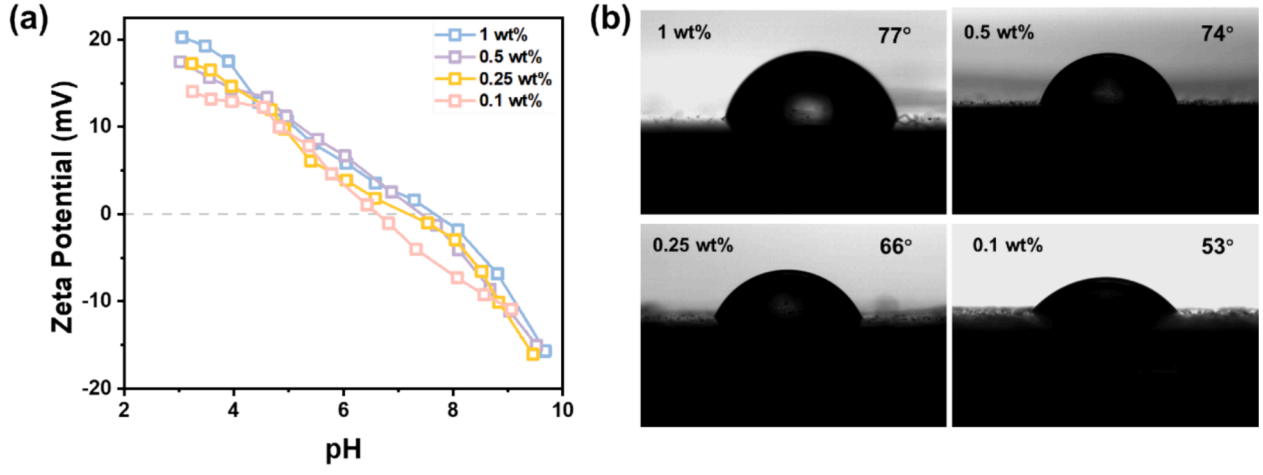

Fig. 3. (a) Surface zeta potential and (b) WCA of the DBH-70 nanowire membranes with different sprayed concentrations at a sprayed volume of 75 μL cm^{-2}.

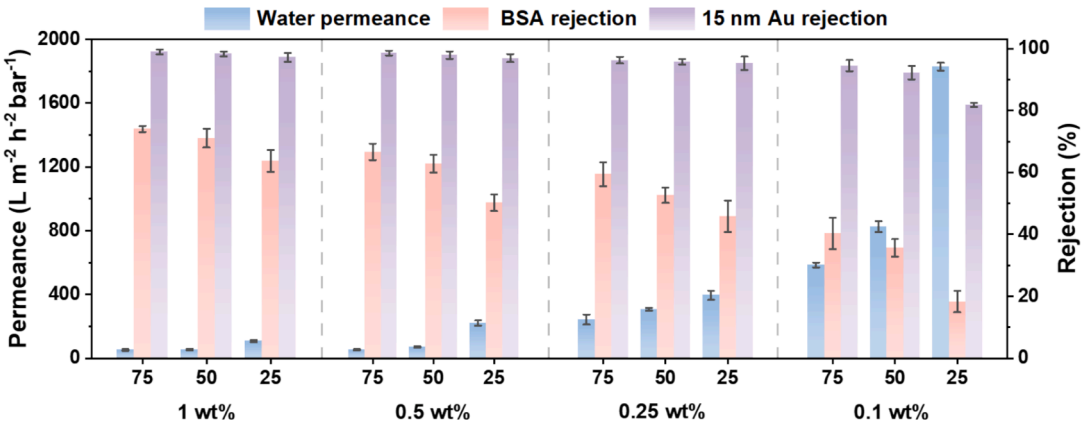

Fig. 4. The water permeances, BSA rejections and 15 nm Au rejections of the DBH-70 nanowire membranes at a series of sprayed concentrations (1–0.1 wt%) and volumes (70–25 μL cm^{-2}).

to BSA in the range of 20 %-75 % by changing the spraying conditions, and the high rejections to gold nanoparticle proved the membrane's outstanding ability to selectively filter substances of varying sizes.

To explore the upscale ability of spray coating, the nanowire membrane with a larger size of 25 cm × 25 cm (Fig. 5a) was prepared at a sprayed concentration of 0.1 wt% and volume of 50 μL cm^{-2} through the same process as above. SEM observation verified the formation of an intact nanowire layer with a thickness of 192 nm (Fig. 5b). The separation performance was tested as shown in Fig. 5c. The water permeance was determined to be 877 L m^{-2} h^{-1} bar^{-1} and the BSA rejection of the membrane was 33 %. The thickness of the nanowire layer as well as the performance of the large-sized membrane were comparable to those of the small-sized membrane. Moreover, separation tests were conducted on four distinct regions of the large-sized membrane, and the result revealed consistent permeance and BSA rejection (Fig. S12), demonstrating the uniformity of the large-sized membrane. From above, the membranes can be flexibly prepared in scalable areas with no expense of performance due to the controllability of additive manufacturing.

4. Conclusions

In this work, the PDMAEMA-*b*-P(BzMA-co-HBMA) BCP nanowires with a high concentration of 20 wt% are prepared through the PISA strategy, and the nanowires, serving as the membrane-forming building block, are subsequently deposited onto macroporous substrates to fabricate ultrafiltration membranes. The morphology and dispersibility

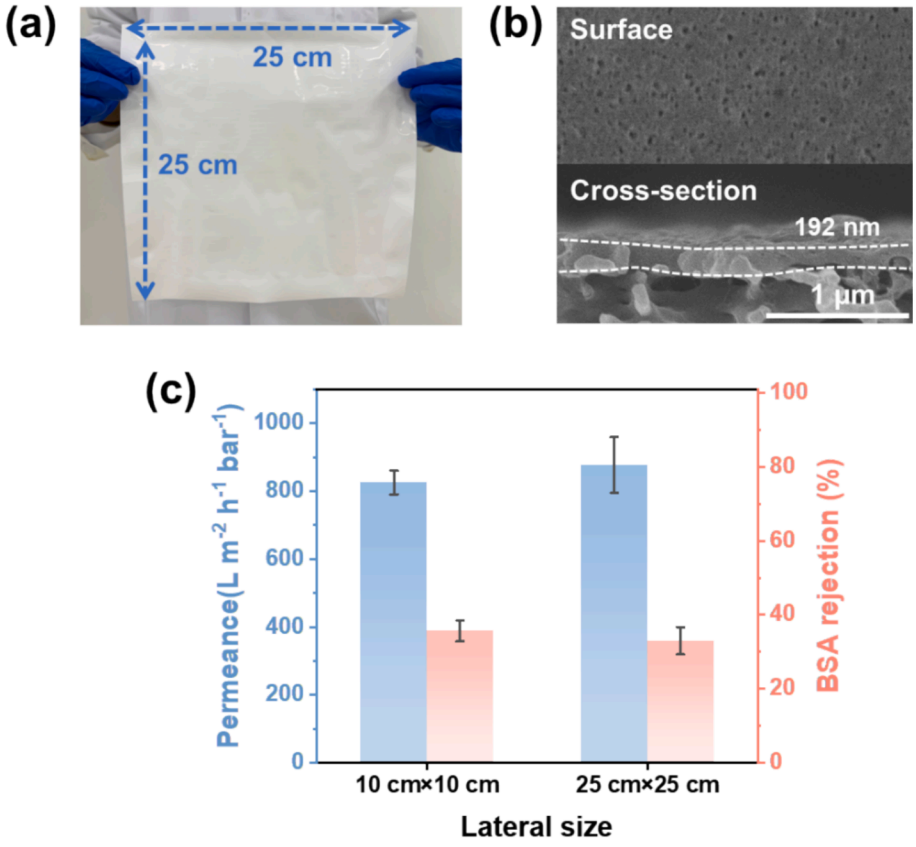

Fig. 5. The nanowire membranes in a larger area prepared with a 0.1 wt% sprayed concentration and 50 μL cm^{-2} sprayed volume: (a) the digital photo, (b) the top surface and cross-sectional SEM images. (c) The comparison of the permeance and BSA rejection of the membranes in large and small areas.

of nanowires depend on the block ratio and DP_{PBzMA}, and experimental results demonstrate that BDH-70 nanowire is optimal for preparing nanowire membranes. By precisely controlling the sprayed concentration and volume of the nanowire, the defect-free thin separation layers are formed with their thicknesses flexibly tunable within a specific range of ~100 nm–3 μm. The controllable membrane architecture allows the resultant membranes to exhibit adjustable properties, boasting permeance ranging from ~50 to 1800 L m^{-2} h^{-1} bar^{-1} and BSA retention varying from ~20 % to 75 %, and the membrane could keep high rejection to 15 nm gold nanoparticles. Moreover, the nanowire membrane with a larger size is prepared, which demonstrates that the strategy presented herein is a controllable and scalable technique, paving the new way for the efficient production of ultrafiltration membranes.

CRediT authorship contribution statement

Jie Deng: Investigation, Data curation, Writing – original draft. **Youxin Gong:** Investigation, Data curation. **Yang Jin:** Validation, Data curation. **Jiemei Zhou:** Methodology, Writing – review & editing, Funding acquisition. **Yong Wang:** Conceptualization, Supervision, Funding acquisition.

Declaration of competing interest

The authors declare that they have no known competing financial interests or personal relationships that could have appeared to influence the work reported in this paper.

Acknowledgments

Financial support from the Natural Science Foundation of Jiangsu Province (BE2022056-3) and the National Natural Science Foundation of China (22478180, 22438005) is gratefully acknowledged.

Appendix A. Supplementary material

Supplementary data to this article can be found online at https://doi.org/10.1016/j.seppur.2025.132980.

Data availability

Data will be made available on request.

References

[1] Y. Hu, M. Yue, F. Yuan, L. Yang, C. Chen, D. Sun, Bio-inspired fabrication of highly permeable and anti-fouling ultrafiltration membranes based on bacterial cellulose for efficient removal of soluble dyes and insoluble oils, J. Membr. Sci. 621 (2021) 118982.
[2] M. Issaoui, S. Jellali, A.A. Zorpas, P. Dutournie, Membrane technology for sustainable water resources management: challenges and future projections, Sustain. Chem. Pharm. 25 (2022) 100590.
[3] U.W.R. Siagian, K. Khoiruddin, A.K. Wardani, P.T.P. Aryanti, I.N. Widiasa, G. Qiu, Y.P. Ting, I.G. Wenten, High-performance ultrafiltration membrane: recent progress and its application for wastewater treatment, Curr. Pollut. Rep. 7 (2021) 448–462.
[4] I. Kammakakam, Z. Lai, Next-generation ultrafiltration membranes: a review of material design, properties, recent progress, and challenges, Chemosphere 316 (2023) 137669.
[5] I. Sadeghi, P. Kaner, A. Asatekin, Controlling and expanding the selectivity of filtration membranes, Chem. Mater. 30 (2018) 7328–7354.
[6] Y. Song, L. Feng, S. Basuray, K.K. Sirkar, S.R. Wickramasinghe, Hemoglobin-BSA separation and purification by internally staged ultrafiltration, Sep. Purif. Technol. 312 (2023) 123363.
[7] S. Fang, H. Tang, M. Wang, Z. Xu, N. Li, The antifouling and separation performance of an ultrafiltration membrane derived from a novel amphiphilic copolymer containing a crown ether, J. Membr. Sci. 676 (2023) 121620.
[8] N. Hampu, J.R. Werber, W.Y. Chan, E.C. Feinberg, M.A. Hillmyer, Next-generation ultrafiltration membranes enabled by block polymers, ACS Nano 14 (2020) 16446–16471.
[9] J.R. Werber, C.O. Osuji, M. Elimelech, Materials for next-generation desalination and water purification membranes, Nat. Rev. Mater. 1 (2016) 16018.
[10] R. Shoshaa, M.Y. Ashfaq, M.A. Al-Ghouti, Recent developments in ultrafiltration membrane technology for the removal of potentially toxic elements, and enhanced antifouling performance: a review, Environ. Technol. Innov. 31 (2023) 103162.
[11] S. Ren, G. Huang, Y. Yao, P. Zhang, Z. Zhang, Y. Wang, Integrating radical polymerization and non-solvent induced phase inversion strategy for functionalized ultrafiltration membrane fabrication, Desalination 573 (2024) 117220.
[12] C. Kahrs, J. Schwellenbach, Membrane formation via non-solvent induced phase separation using sustainable solvents: a comparative study, Polymer 186 (2020) 122071.
[13] M. Pagliero, A. Bottino, A. Comite, C. Costa, Novel hydrophobic PVDF membranes prepared by nonsolvent induced phase separation for membrane distillation, J. Membr. Sci. 596 (2020) 117575.
[14] J.U. Garcia, T. Iwama, E.Y. Chan, D.R. Tree, K.T. Delaney, G.H. Fredrickson, Mechanisms of asymmetric membrane formation in nonsolvent-induced phase separation, ACS Macro Lett. 9 (11) (2020) 1617–1624.
[15] C. Chen, S. Wang, F. Han, X. Zhou, B. Li, A superhydrophilic composite membrane with excellent photo-Fenton antifouling performance for efficient removal of diverse contaminants, Sep. Purif. Technol. 353 (2025) 128380.
[16] Z. Wang, J. Yuan, X. Yang, X. Feng, Y. Zhao, L. Chen, Preparation of PVDF/TMKH-550 composite membrane and its adsorption performance for ammonia nitrogen wastewater, J. Appl. Polym. Sci. 140 (2023) e54396.
[17] Q. Liu, N. Xu, K. Li, Q. Wang, L. Fan, P. Zang, Y. Wan, Enhanced anti-biochemical fouling properties of the polyacrylonitrile membranes assisted by the d-amino acid surface-modified halloysite nanotubes, Chem. Eng. J. 496 (2024) 154285.
[18] D.B. Gutierrez, E.B. Caldona, R.D. Espiritu, R.C. Advincula, The potential of additively manufactured membranes for selective separation and capture of CO_2, MRS Commun. 11 (2021) 391–401.
[19] Y.H. Cheong, L.S. Lai, L. Shi, S.P. Yeap, Y.F. Yeong, W.H. Tay, Z.A. Jawad, Advancing CO_2 separation: exploring the potential of additive manufacturing in membrane technology, Prog. Addit. Manuf. 9 (2024) 2327–2342.
[20] Z.-X. Low, Y.T. Chua, B.M. Ray, D. Mattia, I.S. Metcalfe, D.A. Patterson, Perspective on 3D printing of separation membranes and comparison to related unconventional fabrication techniques, J. Membr. Sci. 523 (2017) 596–613.
[21] X. Qian, M. Ostwal, A. Asatekin, G.M. Geise, Z.P. Smith, W.A. Phillip, R.P. Lively, J. R. McCutcheon, A critical review and commentary on recent progress of additive manufacturing and its impact on membrane technology, J. Membr. Sci. 645 (2022) 120041.
[22] Z. He, C.-P. Hu, H. Chen, X. Chen, S.K.J. Lim, J. Hu, X. Hu, Direct ink writing of geopolymer-based membranes with anisotropic structures for water treatment, J. Membr. Sci. 685 (2023) 121953.
[23] C. Zhang, S. Wang, J. Li, Y. Zhu, T. Peng, H. Yang, Additive manufacturing of products with functional fluid channels: a review, Addit. Manuf. 36 (2020) 101490.
[24] A. Soo, S.M. Ali, H.K. Shon, 3D printing for membrane desalination: challenges and future prospects, Desalination 520 (2021) 115366.
[25] D.W. Ma, Z. Zhang, S. Xiong, J.M. Zhou, Y. Wang, Additive manufacturing of defect-healing polyamide membranes for fast and robust desalination, J. Membr. Sci. 671 (2023) 121407.
[26] M.R. Chowdhury, J. Steffes, B.D. Huey, J.R. McCutcheon, 3D printed polyamide membranes for desalination, Science 361 (2018) 682–685.
[27] X. Geng, J. Wang, J. Ye, S. Yang, Q. Han, H. Lin, F. Liu, Electrosprayed polydopamine membrane: surface morphology, chemical stability and separation performance study, Sep. Purif. Technol. 244 (2020) 116857.
[28] J. Wang, X. Pei, G. Liu, Q. Han, S. Yang, F. Liu, "Living" electrospray – a controllable polydopamine nano-coating strategy with zero liquid discharge for separation, J. Membr. Sci. 586 (2019) 170–176.
[29] D. Ma, H. Li, Z. Meng, C. Zhang, J. Zhou, J. Xia, Y. Wang, Absolute and fast removal of viruses and bacteria from water by spraying-assembled carbon-nanotube membranes, Environ. Sci. Technol. 55 (2021) 15206–15214.
[30] A. Vashishtha, A. Phimphachanh, T. Gaillard, J. Schmitt, C. Gerardin, G. Rydzek, T. Aubert, Hybrid silica cage-type nanostructures made from triply hydrophilic block copolymers single micelles, ACS Nano 18 (2024) 29008–29020.
[31] I.W. Almanassra, L. Jaber, Y. Manawi, M. Sobri Takriff, H. Alawadhi, M. Ali Atieh, M. Ulbricht, Recent advances in 2D materials for improved performance and antifouling characteristics of ultrafiltration membranes, Chem. Eng. J. 488 (2024) 151029.
[32] E.J. Cornel, J. Jiang, S. Chen, J. Du, Principles and characteristics of polymerization-induced self-assembly with various polymerization techniques, CCS Chem. 3 (2021) 2104–2125.
[33] Z. Zhao, S. Lei, M. Zeng, M. Huo, Recent progress in polymerization-induced self-assembly: from the perspective of driving forces, Aggregate 5 (2023) e418.
[34] F. D'Agosto, J. Rieger, M. Lansalot, RAFT-Mediated polymerization-induced self-assembly, Angew. Chem. Int. Ed. 59 (2020) 8368–8392.
[35] S. Zhang, R. Li, Z. An, Degradable block copolymer nanoparticles synthesized by polymerization-induced self-assembly, Angew. Chem. Int. Ed. 63 (2024) e202315849.
[36] J. Wang, M. Cao, P. Zhou, G. Wang, Exploration of a living anionic polymerization mechanism into polymerization-induced self-assembly and site-specific stabilization of the formed nano-objects, Macromolecules 53 (8) (2020) 3157–3165.
[37] P. Wang, N. Li, S. Li, Y. Zhang, Strategies for preparing hybrid nanomaterials via polymerization-induced self-assembly, Eur. Polym. J. 172 (2022) 111234.

[38] M.A.H. Farmer, O.M. Musa, S.P. Armes, Combining crystallization-driven self-assembly with reverse sequence polymerization-induced self-assembly enables the efficient synthesis of hydrolytically degradable anisotropic block copolymer nano-objects directly in concentrated aqueous media, J. Am. Chem. Soc. 146 (24) (2024) 16926–16934.
[39] J. Wan, B. Fan, S.H. Thang, RAFT-mediated polymerization-induced self-assembly (RAFT-PISA): current status and future directions, Chem. Sci. 13 (2022) 4192–4224.
[40] J. Jennings, E.J. Cornel, M.J. Derry, D.L. Beattie, M.J. Rymaruk, O.J. Deane, A. J. Ryan, S.P. Armes, Synthesis of high chi-low n diblock copolymers by polymerization-induced self-assembly, Angew. Chem. Int. Ed. 59 (2020) 10848–10853.
[41] J.I. Calvo, R.I. Peinador, P. Prádanos, L. Palacio, A. Bottino, G. Capannelli, A. Hernández, Liquid–liquid displacement porometry to estimate the molecular weight cut-off of ultrafiltration membranes, Desalination 268 (2011) 174–181.
[42] W.J. Zhang, Z.X. Chang, W. Bai, C.Y. Hong, Greatly enhanced accessibility and reproducibility of worm-like micelles by in situ crosslinking polymerization-induced self-assembly, Angew. Chem. Int. Ed. 61 (43) (2022) e202211792.
[43] Z. Zhang, X. Shi, R. Wang, A. Xiao, Y. Wang, Ultra-permeable polyamide membranes harvested by covalent organic framework nanofiber scaffolds: a two-in-one strategy, Chem. Sci. 10 (39) (2019) 9077–9083.
[44] D.L. Zhong, Z.G. Wang, J.M. Zhou, Y. Wang, Additive-free preparation of hemodialysis membranes from block copolymers of polysulfone and polyethylene glycol, J. Membr. Sci. 618 (2021) 118690.